Interbasin differences in ocean ventilation in response to variations in the Southern Annular Mode

Darryn W. Waugh[1,2*], Kial Stewart[3], Andrew McC. Hogg[3], and Matthew H. England[4]

[1]*Department of Earth and Planetary Sciences, Johns Hopkins University, Baltimore, MD*

[2] *School of Mathematics and Statistics, University of New South Wales, Sydney, New South Wales, Australia*

[3]*Research School of Earth Sciences, and ARC Centre of Excellence for Climate Extremes, Australian National University, Canberra, Australian Capital Territory, Australia*

[4]*Climate Change Research Centre, and ARC Centre of Excellence for Climate Extremes, University of New South Wales, Sydney, New South Wales, Australia*

Corresponding author: Darryn Waugh (waugh@jhu.edu)

Key Points:

- Ventilation of southern oceans in response to changes in the Southern Annular Mode differs between the Pacific Ocean and other basins.
- Large decreases in the ideal age occur in the central Pacific for positive Southern Annular Mode but much smaller changes elsewhere.
- The interbasin differences are due to zonal variations in the wind together with differing ocean responses to increases or shifts in winds.

Abstract

The response of the ventilation of mode and intermediate waters to abrupt changes in the Southern Annular Mode (SAM) is examined by analyzing the ideal age in a global ocean-sea ice model. The age response is shown to differ between the central Pacific Ocean and other basins. In the central Pacific there are large decreases in the age of subtropical mode and intermediate waters associated with a more positive SAM, contrasting only small age changes in the Atlantic and Indian Oceans, except near where intermediate water density surfaces outcrop. These interbasin differences hold for simulations at different horizontal resolutions, and can be explained by the combination of zonal variations in wind stress changes associated with the SAM, and differences in the age response to an increase or shift in the wind stress. These results suggest that the carbon and heat uptake associated with the SAM will likely vary between ocean basins.

Plain Language Summary

The transport of water from the surface into the interior ocean (ocean "ventilation") is an important process in controlling the amount of heat and carbon that is absorbed by the oceans, with impacts on the global climate. We use an ocean – sea ice model to examine how the time scale for the ventilation of the southern subtropical oceans varies with the leading mode of variability of southern hemisphere climate, the so called Southern Annular Mode (SAM). It is shown that there are significant differences between the Pacific Ocean and other basins. In the Pacific there are large decreases in the ventilation time associated with a more positive SAM, but only small changes in the Atlantic and Indian Oceans. This result suggest that the carbon and heat uptake associated with the SAM will likely also vary between ocean basins. The results hold for simulations at different horizontal resolutions, and can be explained by the combination of zonal variations in wind stress changes associated with the SAM, and differences in the ventilation response to an increase or shift in the wind stress.

1 Introduction

The Southern Annular Mode (SAM) is the dominant mode of circulation variability in southern mid and high latitude atmosphere and oceans (e.g., Thompson and Wallace 2000, Marshall et al. 2004), and there has been a positive trend in SAM over the last four decades (e.g., Thompson and Solomon 2002). Associated with this trend there has been an intensification and poleward shift of the zonally averaged westerly winds during summer, which is linked to a range of changes in the ocean circulation, including enhanced Ekman transport with increased upwelling in mid-latitudes and downwelling at high latitudes (e.g., Hall and Visbeck 2002; Sen Gupta and England 2006), and an increase, via Sverdrup balance, in the horizontal circulation and strength of the subtropical gyres (e.g., Cai et al. 2006, Roemmich et al. 2007). These changes in ocean circulation then have an impact on the ocean heat and carbon content, the Antarctic Circumpolar Current, ventilation ages, and mode water properties (e.g., Boning et al 2008, Cai et al. 2010, Le Quéré et al., 2007, Waugh et al. 2013, Ting and Holzer 2017, Gao et al. 2018).

Although changes in a wide range of ocean aspects have been linked to changes in SAM, a quantitative relationship is generally lacking. Furthermore, much of the focus has been on changes in zonally averaged winds and ocean circulation: While the SAM is predominantly zonally symmetric there are zonal variations in the strength and meridional structure of the westerly winds associated with SAM during winter (e.g., Codron 2007, Fogt et al. 2012) that could introduce zonal asymmetries in the oceanic response. Zonal asymmetry arguably has a greater impact on the ocean than in the atmosphere, owing to the nature of circulation within closed ocean basins north of 35°S, and the strong bathymetric steering of flow in the ACC via conservation of potential vorticity.

Here we examine the zonally-varying impact of the SAM on the ventilation of Subantarctic Mode Water (SAMW) and Antarctic Intermediate Water (AAIW). The ventilation of these waters is an important control of the ocean uptake of heat and carbon as well as ocean nutrients (e.g. Frolicher et al. 2015), and knowledge of the ventilation response to SAM will shed light on the potential impact on these processes. The ventilation within the model is quantified using the ideal age, which is not only a fundamental measure of the ventilation but also can be used as a proxy for changes in ocean heat or carbon uptake (e.g. Russell et al. 2006).

Several previous modeling studies have examined the change in ideal age for an increase and poleward shift in the wind stress, either in response to increased atmospheric CO_2 (e.g., Bryan 2006, Ganadesikan et al. 2007) or due to idealized wind perturbations (e.g., Farneti and Gent 2011, Waugh 2014, Waugh et al. 2019). These studies have shown a general decrease in the ideal age (i.e. more rapid ventilation) in SAMW/AAIW when there is an increase and poleward shift in the wind. However, they have considered only the zonal-mean age response or zonally symmetric wind perturbations. As discussed above the changes in the wind stresses accompanying a change in SAM are not zonally uniform, but the impact of these zonal variations on the age response has not been examined. This is the focus of this study.

We examine the age response in a suite of ocean-sea ice model simulations with an abrupt change in the atmospheric forcing from a year with neutral SAM to a year with extreme anomalous positive or negative SAM (Stewart et al 2020a). These abrupt change in forcing simulations enable the response to be a particular anomalous SAM to be isolated. It is difficult to isolate the response to a particular SAM event from simulations with interannually varying forcing, as the response time for the ideal age to changes in atmospheric forcing is multiple decades and ocean changes

are due to the time-integrated (weighted) change in the atmospheric forcing (Waugh and Haine 2020) and hence to several different phases of SAM.

The model simulations analyzed and methods used are described in the next Section. Then, before examining the perturbation experiments, we quantify in Section 3 the relationships between SAM and wind stress over the southern oceans. The zonal-mean age response is examined in Section 4, while regional variations (in particular, differences between oceans) are examined in Section 5. Concluding remarks are in the final section.

2. Model and Methods

We examine a suite of simulations using the Australian Community Climate and Earth System Simulator, ocean model version 2 (ACCESS-OM2) global ocean-sea ice model (Kiss et al. 2020) where atmospheric forcing for different 12-month periods from the Japanese 55-year atmospheric reanalysis data-set for driving ocean models (JRA55-do, Tsujino et al., 2018) are used repeatedly to drive the model (Stewart et al 2020a). This suite includes simulations using 12-month periods previously identified as globally climatically-neutral periods suitable for extended simulations without interannual variability or substantial model drift (Stewart et al., 2020b), as well as 12-month periods with extremely anomalous (positive and negative) Southern Annular Mode (SAM) conditions (Stewart et al. 2020a). The latter are referred to as "SAM+ years" (for extreme positive SAM periods) and "SAM- years".

These simulations have been performed at three different resolutions (nominal horizontal resolution of 1°, 0.25° and 0.1°. We focus here on the 1° version as three different reference year simulations have been performed, and for each there are six perturbation simulations (three SAM+ and three SAM-). For the higher resolution simulations there is only a single reference case, and four SAM perturbations (two SAM+ and two SAM-) (Stewart et al. 2020a).

The 1° version of ACCESS-OM2 has a horizontal grid spacing of (nominally) 1° latitude and longitude, and 50 unevenly spaced vertical levels in a z* generalized vertical coordinate. The vertical grid spacing increases smoothly with depth from 2.3m at the surface to ~220m at ~3000m (maximum depth of ~5400m), designed to support the vertical structure of mode-1 baroclinic processes (Stewart et al. 2017). See Kiss et al (2020) for additional model details and evaluation.

Reference year simulations with the 1° model version have been performed with 12-month (May to April of the following year) periods from 1984/85, 1990/91 and 2003/04 (referred to as RYF8485, RYF9091 and RYF0304). These simulations were initialized with January temperature and salinity fields from the World Ocean Atlas 2013 (WOA13; Locarnini et al., 2013; Zweng et al., 2013) and run for 600 years. For each of the three 600-year RYF simulations, eight 300-year perturbations are branched off at the model year 300. Two of these perturbations correspond to the other two RYF periods and six correspond to SAM periods: The SAM+ years are 1998/99, 2010/11 and 2015/16 (referred to as SAM+9899, SAM+1011, and SAM+1516, respectively), and the SAM- years are 1991/92, 2003/04 and 2016/17 (referred to as SAM-9192, SAM-0304 and SAM-1617, respectively). In these perturbation simulations the atmospheric forcing fields used to calculate air-sea fluxes are abruptly changed from the RYF to the different forcing without smoothing. This approach grants a total of 27 simulations; 3x 600-year RYF simulations, and 24x 300-year perturbation simulations.

The three RYF periods and six extreme SAM periods represent nine different forcing years with a range of SAM conditions. The three RYF periods, while not identified based on the neutrality of SAM alone, have near neutral SAM indices. This is evident in the latitudinal variation

of anomalies in (a) sea-level pressure and (b) zonal-mean winds, shown in **Figure 1**. The three reference years (green curves) generally have small anomalies in SLP and winds. The SAM+ years (red) have positive SLP anomalies at lower latitude and negative SLP anomalies at high latitudes, which correspond to positive wind anomalies south of 45ºS. The SAM- years (blue) generally have the opposite SLP and wind anomalies to the positive years. The years RYF8485 and SAM-1617 do not fit exactly in the above characterization, as the SAM anomaly for RYF8485 (SAM=-0.37) is more negative than SAM-1617 (SAM=-0.10).

All simulations include an ideal age tracer diagnostic (or "age" for short). This tracer is set to zero in the model surface level (which is 2.3m thick) at each time step, increases by 1 yr yr^{-1} within the ocean interior, and is advected and diffused as other tracers (e.g., temperature and salinity). In the limit of long times compared to the circulation, the ideal age equals the mean time since water last made surface contact (e.g., England 1995, Hall and Haine 2002). Waugh et al. (2019) examined the change in ideal age in wind stress perturbation simulations with an early (0.25º) version of MOM.

We focus on the age distribution for $\sigma_2 < 36.5$ kg/m^3, which includes SAMW and AAIW, as the ventilation of these waters is particularly important for understanding the ocean uptake of heat and carbon. The majority of our analysis is on fields averaged over the last 10 years of the perturbation simulations (i.e. 290-299 years after the perturbation was applied), and the difference in these average fields from corresponding averaged in the RYF simulations.

3. Relationship between SAM and wind stress

The primary mechanism by which changes in SAM are thought to influence the ocean circulation and ventilation is through changes in the wind stress. Therefore, before examining the age in the perturbation experiments described above we quantify the relationship between SAM and zonal wind stress (τ_x). For this analysis we use the SAM index and wind stress for 1979/80 to 2016/17 from an ACCESS-OM2 simulation driven by interannual JRA55-do atmospheric state from 1958 to 2017 (IAF; Kiss et al., 2020). This IAF simulation was continuously cycled through five iterations of this forcing dataset, and we analyze the model output from the last cycle. For both SAM and wind stress we examine the annual-mean from 1 May to 30 April the following year.

A linear regression analysis between τ_x and SAM shows that there is generally an increase in the τ_x poleward of 45ºS (with peak increase around 55ºS) and decrease equatorward of 45ºS for positive SAM (**Figure 2**). As the climatological peak τ_x at each longitude is around 50-55ºS (bold curve), the polar increase and mid-latitude decrease of τ_x corresponds to an increase and poleward shift of the peak zonal-mean τ_x with a more positive SAM. This poleward intensification is shown more clearly in **Figs. 3a,b** which show that both magnitude and latitude of the peak zonal-mean τ_x are highly correlated with SAM (correlation coefficient r=0.9 and r=-0.7, respectively. There are, however, substantial zonal variations in the latitude of the peak zonal wind stress, with peak values of τ_x over the Pacific poleward of those over the Atlantic and Indian oceans (thick curve in **Fig 2**), and the relationship between SAM and the magnitude and latitude of the peak τ_x varies with longitude.

The relationship between the SAM index and the magnitude and latitude of the peak τ_x averaged over the Pacific Ocean (150ºE-70ºW) and the combined Atlantic and Indian Oceans

(60°W-120°E) is quantified in **Figs 3c-f**[1]. The SAM–τ_x relationships differ between the Pacific and Atlantic-Indian Oceans. The magnitude of the peak τ_x averaged over the Pacific is highly correlated with SAM (r=0.9), but there are insignificant correlations between the latitude of the peak τ_x and SAM (r=0.1). In contrast, the latitude and magnitude of the peak Atlantic-Indian τ_x are both correlated with SAM (but slightly weaker than the peak Pacific τ_x). These differences in SAM-τ_x relationships between the Pacific and Atlantic-Indian oceans are consistent with previous studies of the zonal asymmetries in SAM (e.g. Codron 2007, Fogt et al. 2012).

4. Zonal-Mean Age Response

The above differences in the SAM – wind stress relationship between basins suggests that the ocean response to SAM could vary between basins. However, before examining the age response in different basins we first examine the zonal-mean age response, principally to allow comparison with previous studies examining the zonal-mean age response to changes in wind stress.

Figure 4 shows that there are substantial changes in the zonal-mean age response ($\Delta\bar{a}$) for the SAM+ and SAM- perturbations from the RYF9091 simulations, with maximum age changes of 30-50%. There is a wide variation in the spatial pattern and sign of $\Delta\bar{a}$: For some perturbations the sign of $\Delta\bar{a}$ is the same throughout nearly all of the mode and intermediate waters (35.5 kg/m^3 < σ_2 < 36.5) (e.g., **Fig 4a,b, f**), while for other perturbations there are both regions of increase and decrease in $\Delta\bar{a}$ within these waters (e.g., **Fig 4d,e).**

Much of the variation among the perturbations in $\Delta\bar{a}$ within SAMW and AAIW can be explained by differences in the SAM anomaly (ΔSAM; see value listed at the bottom of each panel in **Fig 4**). There is a decrease in age throughout most of the mode-intermediate waters for perturbations with ΔSAM>0 and an increase in age when ΔSAM<0. However, the SAM anomaly is not the sole determinant, as there are differences between the response for perturbations with the same or similar SAM (e.g. 9899 and 1011). Also, for all perturbations $\Delta\bar{a} < 0$ at the location 35°S, 500 m depth (σ_2 = 35.5 kg/m^3). In this region $\Delta\bar{a}$ is insensitive to ΔSAM.

To quantify the change in age associated with SAM we perform a linear regression analysis using $\Delta\bar{a}$ from the perturbation simulations branching off a given RYF simulation and corresponding changes in ΔSAM. That is, at a given latitude (φ) and depth (z), we solve for α_{SAM},

$$\Delta\bar{a}_k(\varphi, z) = \alpha_{SAM}(\varphi, z)\Delta SAM_k + c, \qquad (1)$$

where ΔSAM_k is the change in SAM index for the kth perturbation, $\Delta\bar{a}_k$ the age response for corresponding perturbation, c is a constant, and α_{SAM} is the sensitivity of $\bar{a}$ to a unit change in the SAM index. This regression is performed over the perturbations from all three RYF simulations (i.e. over 24 perturbation simulations). As shown in **Fig. 5a**, there is a decrease in $\bar{a}$ with increasing SAM (negative α_{SAM}) throughout AAIW and in lower parts of SAMW. In the upper part of SAMW and lighter waters α_{SAM} is small and there is not a significant correlation between SAM and $\bar{a}$. The largest percentage difference occurs in AAIW around 50-55°S, where α_{SAM} ~ -50% per unit SAM.

[1] Analysis of interannual correlations of latitude and magnitude of the peak winds averaged over different oceans shows a high correlation between the Atlantic and Indian Oceans, but only weak interannual correlations between Pacific-average wind stress and wind stress over Atlantic or Indian Oceans.

As shown above there is a high correlation between both the change in magnitude of the peak zonal wind stress (τ_{max}) and the change in latitude of this peak (τ_{lat}) with the change in SAM. The decrease in mode and intermediate water age with SAM is therefore consistent with previous studies showing a decrease in age for increased and poleward shifted winds (e.g., Waugh et al. 2019). To isolate the role of an increase or shift in the wind stress governing changes in the zonal-mean age we apply a multiple linear regression analysis similar to the above SAM analysis, i.e. at each latitude and depth, we solve for $\alpha_{increase}$ and α_{shift} in the set of equations

$$\Delta\bar{a}_k(\varphi, z) = \alpha_{increase}(\varphi, z)\Delta\tau_{max,k} - \alpha_{shift}(\varphi, z)\Delta\tau_{lat,k} + c \qquad (2)$$

where $\Delta\tau_{max,k}$ and $\Delta\tau_{lat,k}$ are changes in magnitude and location of peak wind stress for the kth perturbation, and the quantities $\alpha_{increase}$ and α_{shift} correspond to the sensitivity of the age to an increase and a shift in the peak wind stress, respectively. There is a negative sign before the second term so that a positive α_{shift} indicates the sensitivity to a poleward shift in the peak wind stresses. There is a decrease in age throughout mode and intermediate waters (35.5 kg/m^3 < σ_2 < 36.5) for an increase in the wind stress (**Figure 5b)**. On the other hand, age decreases only poleward of 45^{o}S for a poleward shift in the peak wind stress, and there is (statistically insignificant) increase of age equatorward of 45^{o}S (**Figure 5c)**.

The range of τ_{max} across the perturbations is around 0.05 N/m^2 while the range of τ_{lat} is around 3^o (see **Fig 3**). Combining these ranges with maximum magnitude of $\alpha_{increase}$ and α_{shift} (15% per 0.01 N/m^2 and 25% per degree, respectively) indicates that the peak changes of $\Delta\bar{a}$ associated with an increase or shift of wind stresses are of similar magnitude. Thus, both the increase and shift of the peak wind stress needs to be considered. Although, as the maximum contributions from an increase or shift in winds occur in different locations, the relative importance of an increase or shift is expected to vary zonally.

The spatial patterns of $\alpha_{increase}$, and α_{shift} in **Fig 5** are similar to those from the abrupt wind-stress perturbations shown in Waugh et al. (2019). This similarity also applies to the magnitude of the response. **Figure 6(a,b)** shows the results of the multiple linear regression analysis of RYF9091 perturbations 50 years after the perturbation (to be consistent with the length of the simulations in Waugh et al. (2019)). These results are compared (in **Fig 6c,d**) with Δa from the Waugh et al. (2019) simulations re-expressed as sensitivities $\alpha_{increase}$ and α_{shift}. Note that the smaller magnitude of $\alpha_{increase}$ for 50 years, rather than 300 years after the perturbation, is consistent with decadal-to-century age response time shown in Waugh and Haine (2020). Figure 6 shows good agreement between the estimated and directly simulated (Waugh et al. 2019) sensitivities, including the spatial structure and magnitude of the sensitivities. Note, although the region of positive α_{shift} in Fig 5c is not statistically significant, the direct simulations also shows positive α_{shift} at lower latitudes. The good agreement in **Fig 6** is perhaps surprising given the many differences between the two sets of simulations: The sensitivities in Waugh et al. (2019) come from direct perturbations and not a regression analysis, and the Waugh et al. (2019) simulations have zonally symmetric wind perturbations, with no seasonality, and no changes in other atmospheric properties (e.g., buoyancy fluxes). The overall agreement supports the conclusion that changes in zonal-mean ideal age within southern mode and intermediate waters in response to abrupt change in SAM are consistent with response to changes in magnitude and latitude of the peak zonal-mean wind stress.

5. Zonal Variations in Age Response

The above analysis has shown that the zonal-mean ideal age response is consistent with expected changes from the change in zonal-mean wind stress between simulations, however, the analysis in Section 3 shows large differences in the SAM-wind stress relationship between the Pacific and Atlantic-Indian oceans. Thus, differences in the age response between ocean basins may be expected.

Substantial zonal variation in the age response at fixed depth are indeed found (see **Figure 7**). This variation is not limited to the magnitude of Δa; for many perturbations the sign of Δa changes with longitude. In some simulations the sign of subtropical (30-45ºS) central Pacific Δa differs from the subtropical Δa in the Indian and/or Atlantic Oceans (e.g., **Fig 7a,e,f**). In other cases, the sign of the central Pacific Δa differs from that in the Tasman Sea and the eastern boundary of the Pacific Ocean (e.g., **Fig 7c,e**). Furthermore, there is an age decrease in the Tasman Sea for all perturbation simulations (i.e. changes independent of the sign the change in SAM).

To quantify these zonal variations, we examined the relationships among 30-45°S Δa averaged over the Central Pacific (170-100°W), Indian (30-120°E), Atlantic (60°W-20°E), Eastern Pacific Oceans (80-70°W), or the Tasman Sea (155-165°E). For Δa at 900 m, there is only a very weak relationship between the Central Pacific Δa and either the Indian or Atlantic Oceans Δa (correlation coefficient, r, equal 0.2 and 0.4 respectively). Further, there is also only a very weak relationship between the Central Pacific Δa and that over the Eastern Pacific or Tasman Sea (r = 0.4, 0.2, respectively). In contrast, there is a high correlation between the Indian and Atlantic Ocean Δa (r=0.96), between Indian Ocean and Tasman Sea Δa (r=0.65), and between the Atlantic Ocean and Eastern Pacific Δa (r=0.91).

Waugh et al. (2019) showed that much of the zonal-mean age response within SAMW and AAIW can be explained by a change in subtropical gyre transport induced by the change in wind stress curl, consistent with Sverdrup balance. This relationship also applies to the simulations considered here, only now we assess more carefully the inter-basin differences. The changes in barotropic stream function (BSF) calculated from Sverdrup balance for the perturbation from RYF9091 are shown in **Figure 8** and are consistent with many of the features in maps of 900m Δa shown in **Fig 7**. For example, the sign of Δa within the central Pacific is the same as that of the ΔBSF, consistent with an increase in BSF corresponding to a weaker barotropic circulation (the BSF is negative within the southern subtropical gyres) which leads to slower advection of water and older ages. Also, there are generally differences in the pattern (and sign) of ΔBSF in the Pacific from the Atlantic and Indian Oceans, consistent with the differences in Δa between oceans. There are also perturbations where the sign of ΔBSF in the central Pacific differs from the eastern Pacific or Tasman Sea.

The differences in Δa between basins are not limited to 900m, but occur throughout mode and intermediate waters. As illustrated in **Fig 9** for a SAM+ and SAM- perturbation, there are large changes in the Central Pacific age in mid-latitude (30-45ºS) SAMW and AAIW with SAM, with age increasing (decreasing) by around 30-40% for a decrease (increase) in SAM. In contrast, for age averaged over the Atlantic-Indian Oceans there are only small changes in mid-latitudes that are often of opposite sign from the Central Pacific, and the largest change in the Atlantic-Indian Oceans occur further south in near-surface AAIW.

Figure 9 indicates that the age-SAM relationship is very different between the Central Pacific and Atlantic-Indian average age. To quantify this, we perform the age-SAM linear regression analysis (equation 1) for the basin-average rather than zonal-mean a. As shown in **Fig**

10a,d, there is negative α_{SAM} (a decrease in age for increase in SAM) for both the Central Pacific and Atlantic-Indian oceans, but the magnitude and spatial structure differs. There are large positive values of Central Pacific α_{SAM} in subtropical SAMW and AAIW (30-50^{o}S, $35.5 < \sigma_2 < 36.5$ kg/m^3) with, and smaller, generally insignificant, values elsewhere. In contrast, α_{SAM} is small (insignificant) for Atlantic-Indian age in this region, and large α_{SAM} are limited to more southern AAIW (~55^{o}S, σ_2 ~ 36.5 kg/m^3) near the surface (and the decrease in age is smaller, with peak around 30-40% per unit of SAM).

The above differences in age response to SAM between basins are consistent with the combination of (i) inter-basins differences in wind stress changes associated with SAM and (ii) the different age response to an increase or shift in peak wind stress. Over the Pacific the magnitude of τ is positively correlated with SAM but there is no correlation between the location of peak τ and SAM (Section 3). We therefore expect the age change associated with SAM in the Pacific Ocean to mirror the response to an increase in wind stress, which is a decrease in age in subtropical SAMW and AAIW waters (Section 4). This decrease is indeed what **Fig 10a** shows. For the Atlantic-Indian Oceans there is both an increase and poleward shift in wind stress associated with positive SAM (Fig 3), and both impact the age. North of 45^{o}S (within 500-1000 m) the age decreases with an increase of the peak wind stress (**Fig 5**) but age increases with a poleward shift, so these wind stress changes cancel each other and little change in *a* with SAM is expected (consistent with **Fig 10b**). South of 45^{o}S a poleward shift in peak wind stress cause the opposite sign change in age. Thus, both an increase and shift associated with SAM cause a decrease in age, again consistent with **Fig 10b**.

6. Resolution Dependence

A possible concern with the results presented above is the low horizontal resolution (1^o) of the model, which raises the question as to whether the impact of mesoscale eddies is accurately captured. As described in Section 2, some simulations at 0.25° and 0.1° horizontal resolution have also been performed, and we now use output from these simulations to assess the impact of horizontal resolution on the age response and our key conclusions.

For the higher resolution simulations there is only a single (RYF9091) reference case, and the perturbation simulations were branched from year 150 (0.25° resolution) and year 50 (0.1° resolution), rather than year 300 in the 1° resolution (Stewart et al 2020a). Furthermore, only four perturbation simulations were performed, and the 0.1° perturbations were only run for 20 years. Thus, the full analysis described above cannot be repeated for the higher resolution runs. However, the response for individual perturbations can be compared. As there is a decadal to centennial response time for age to wind stress perturbations (Waugh and Haine 2020), it is important to compare simulations are at same stage of the transient response. Thus, we compare simulations 20 years (the length of the 0.1° simulations) after the perturbation was applied. This comparison is shown in **Figure 11** which shows the ideal age response, averaged over the Central Pacific or Atlantic-Indian oceans, for the SAM-9192 and SAM+9899 perturbations from RYF9091, for 1.0^o, 0.25^o and 0.1^o resolution simulations. The 1^o simulations in **Figure 11** are the same as in **Figure 9**, but for an earlier response time (20 instead of 300 yrs).

The broad scale patterns and magnitude of the response shown in **Figure 11** are the same for all resolutions. In particular, for all resolutions there is a much larger response in the Central Pacific (maximum around 20-30%) than in the Atlantic-Indian Oceans (generally around or less than 5%).

There are some differences in detail between the different resolutions, with the most noticeable being a shallower response in the Central Pacific at the higher resolution. The cause of this difference is unclear. It is most likely related to a more realistic, along-isopycnal eddy transport at higher resolution (Stewart et al 2020a). Further research is required to determine the cause of the shallower response at the higher resolution, but this difference does not impact our primary conclusion that the age-SAM relationship differs between the Central Pacific and Atlantic-Indian Oceans.

The limited sensitivity of the age response to resolution shown in Figure 11 is consistent with the agreement in the simulated age response to an increase in the zonal-mean winds from 1° coupled climate model (Waugh 2014) and 0.25° ocean-sea ice model (Waugh et al 2019) simulations. Furthermore, it is also consistent with the Waugh et al (2019) result that the change in age can be explained by the change in wind stress curl and linear theory, i.e. age changes due a combination of vertical movement of isopycnals (via Ekman pumping) and changes in horizontal circulation (via Sverdrup balance).

7. Conclusions

Analysis of a suite of abrupt forcing simulations with the ACCESS-OM2 ocean-sea ice model indicates that the response of the ventilation of southern mode and intermediate waters (SAMW/AAIW) to changes in SAM differs between the central Pacific Ocean and other basins. In the Central Pacific there are large decreases in the ideal age in subtropical SAMW/AAIW associated with a more positive SAM, and smaller, generally insignificant, changes elsewhere. In contrast, in the Atlantic-Indian Oceans the age decreases associated with an increase in SAM are small except in more polar, near-surface AAIW. The conclusion that the age response to SAM is much larger in the Central Pacific than in other ocean basins is not sensitive to the horizontal resolution of the simulations, and the holds for simulations at 1°, 0.25° and 0.1°.

These inter-basin differences in age response are due to the combination of zonal variations in the changes in wind stress associated with an increase in SAM, together with the different age response to an increase or shift in the peak wind stress. Over the Pacific Ocean the magnitude of the peak wind stress is highly correlated with SAM, but there are insignificant correlations between the latitude of the peak wind stress and SAM. The decrease of age in SAMW and AAIW within the Central Pacific is consistent with this increase in wind stress (with limited shift) associated with SAM. In contrast, both the latitude and magnitude of the peak Atlantic-Indian wind stress are correlated with SAM, and large changes in age are limited to south of 45°S as the increase and poleward shift of the wind stress cause opposing age changes north of 45°N.

The atmospheric forcing used for the different SAM+ or SAM- perturbations include differences not only in the wind stress but also in buoyancy fluxes, and changes in buoyancy fluxes could contribute to the differences in age. It is not possible from these simulations to isolate the role of wind versus buoyancy forcing, but the ability of the wind stress changes associated with SAM (and linear theory) to explain the SAMW/AAIW age changes indicates that changes in buoyancy fluxes play only a minor role in the age-SAM relationship. This minor role may not carry over to all aspects of the ocean response, i.e. changes in mixed layer depth and subduction rates are likely more sensitive to SAM-related changes in buoyancy fluxes (Downes et al. 2017, Sallee et al. 2010).

One question that follows the above modeling results is whether there is observational evidence for regional variations in ocean ventilation associated with SAM. A direct comparison of the simulations examined here and observations is not possible given that we have analyzed the

long-term (steady) response in idealized (unrealistic) abrupt forcing simulations, whereas in reality there are interannual variations in atmospheric forcing and the age responds to the time-integrated changes in wind stress over previous decades (Waugh and Haine 2020). However, the simulations may provide guidance for the age response to the positive trend in SAM over the last four decades. Analysis of repeat measurements of transient tracers in the southern oceans by Waugh et al. (2013) and Ting and Holzer (2017) show a decrease in SAMW age from the early 1990s to mid 2000s within all three ocean basins. This would appear to contradict the model result which indicates there should a substantial decrease of age in subtropical SAMW within the Central Pacific, but much smaller age changes in corresponding water within the Atlantic/Indian Oceans. However, the observational estimates in the Indian and Atlantic Oceans is based on a single section in each ocean (as opposed to 3 in the Pacific) and the estimated changes in age are noisy (less coherent) than in the Pacific Ocean. Furthermore, analysis of a different (zonal) section in the southern Indian Ocean by Álvarez et al (2011) and Tanhua et al. (2013) indicate no long-term change in the age. Thus, it is possible that changes in SAMW age have been much larger across the central Pacific Ocean than averaged over the Indian Ocean. Further analysis required to test this, including analysis of more recent repeat transient tracer measurements.

Another area worth pursing is the possible connection between inter-basin differences in the age response to SAM and the oceanic uptake of carbon and heat. For example, Keppler and Landschützer (2019) have shown regional differences in the carbon uptake associated with SAM, and whether this can be explained by the inter-basin differences in wind stress and age relationships with SAM needs to be explored.

Acknowledgments

The ACCESS-OM2 model output is in the process of being uploaded to the COSIMA Model Output Collection; when this process is complete the data will be available from doi: 10.4225/41/5a2dc8543105a. This work was supported by computational resources provided by the Australian Government through the National Computational Infrastructure, Canberra.

References

Álvarez, M., Tanhua, T., Brix, H., Lo Monaco, C., Metzl, N., McDonagh, E. L., & Bryden, H. L. (2011). Decadal biogeochemical changes in the subtropical Indian Ocean associated with Subantarctic Mode Water. *Journal of Geophysical Research: Oceans*, *116*(C9).

Böning C. W., Dispert, A., Visbeck, M., Rintoul, S. R. & Schwarzkopf, F. U. 2008: The response of the Antarctic Circumpolar Current to recent climate change. *Nature Geosci*. 1, 864-869.

Bryan, F. O., Danabasoglu, G., Nakashiki, N., Yoshida, Y., Kim, D. H., Tsutsui, J., & Doney, S. C. (2006). Response of the North Atlantic thermohaline circulation and ventilation to increasing carbon dioxide in CCSM3. *Journal of Climate*, *19*(11), 2382-2397.

Cai, W. (2006). Antarctic ozone depletion causes an intensification of the Southern Ocean super-gyre circulation. *Geophysical Research Letters*, *33*(3).

Cai W, Cowan T, Godfrey S, Wijffels S (2010), Simulation of processes associated with the fast warming rate of the southern midlatitude ocean. *J Climate*, 23:197–206

Codron, F. (2007). Relations between annular modes and the mean state: Southern Hemisphere winter. *Journal of the atmospheric sciences*, *64*(9), 3328-3339.

Downes, S. M., C. Langlais, J. P. Brook, & P. Spence (2017). Regional impacts of the westerly winds on Southern Ocean Mode and Intermediate Water subduction. *J. Phys. Oceanogr*., 47, 2521–2530.

England, M.H., (1995). The age of water and ventilation timescales in a global ocean model. *J Phys. Oceanogr.*, *25*, 2756-2777.

Fogt, R. L., Jones, J. M., & Renwick, J. (2012). Seasonal zonal asymmetries in the Southern Annular Mode and their impact on regional temperature anomalies. *Journal of climate*, *25*(18), 6253-6270.

Frölicher, T. L., Sarmiento, J. L., Paynter, D. J., Dunne, J. P., Krasting, J. P., & Winton, M., (2015). Dominance of the Southern Ocean in Anthropogenic Carbon and Heat Uptake in CMIP5 Models. Journal of Climate, 28(2), 862–886, doi: 10.1175/JCLI-D-14-00117.1.

Farneti, R., and P. R. Gent (2011). The effects of the eddy-induced advection coefficient in a coarse-resolution coupled climate model. Ocean Modell., 39, 135–145, https://doi.org/10.1016/ j.ocemod.2011.02.005.

Gnanadesikan, A., Russell, J. L., & Zeng, F. (2007). How does ocean ventilation change under global warming? Ocean Sci., 3, 43–53.

Gao, L., Rintoul, S.R. & Yu, W., 2018. Recent wind-driven change in Subantarctic Mode Water and its impact on ocean heat storage. *Nature Climate Change*, *8*, 58.

Hall, A. and Visbeck, M., (2002), Synchronous variability in the Southern Hemisphere atmosphere, sea ice, and ocean resulting from the annular mode. *Journal of Climate*, *15*(21), pp.3043-3057

Hall, T.M., & T.W.N. Haine 2002: On Ocean Transport Diagnostics: The Idealized Age Tracer and the Age Spectrum, *J. Phys. Ocean.*, 1987-2001.

Keppler, L., & Landschützer, P. (2019). Regional wind variability modulates the Southern Ocean carbon sink. *Scientific reports*, *9*(1), 1-10.

Kiss, A. E., Hogg, A. McC., Hannah, N., Boeira Dias, F., Brassington, G. B., Chamberlain, M. A., Chapman, C., Dobrohotoff, P., Domingues, C. M., Duran, E. R., England, M. H., Fiedler, R., Griffies, S. M., Heerdegen, A., Heil, P., Holmes, R. M., Klocker, A., Marsland, S. J., Morrison, A. K., Munroe, J., Nikurashin, M., Oke, P. R., Pilo, G. S., Richet, O., Savita, A., Spence, P., Stewart, K. D., Ward, M. L., Wu, F., and Zhang, X., (2020). ACCESS-OM2

v1.0: a global ocean–sea ice model at three resolutions, *Geosci. Model Dev*., 13, 401–442, doi:10.5194/gmd-13-401-2020.

Le Quéré, C., Rödenbeck, C., Buitenhuis, E.T., Conway, T.J., Langenfelds, R., Gomez, A., Labuschagne, C.Ramonet, M., Nakazawa, T., Metzl, N. & Gillett, N. (2007). Saturation of the Southern Ocean CO2 sink due to recent climate change. Science, 316, 1735-1738

Marshall, G. J., Stott, P. A., Turner, J., Connolley, W. M., King, J. C., & Lachlan-Cope, T. A. (2004). Causes of exceptional atmospheric circulation changes in the Southern Hemisphere. *Geophysical Research Letters*, *31*(14).

Roemmich, D., J Gilson, R. Davis, P. Sutton, S. Wijffels, & S. Riser, (2007). Decadal Spinup of the South Pacific Subtropical Gyre, J. Phys. Ocean., 37, 162.

Roemmich, D., Gilson, J., Sutton, P. & Zilberman, N., (2016). Multidecadal change of the South Pacific gyre circulation. *Journal of Physical Oceanography*, *46*(6), pp.1871-1883.

Russell, J.L., Dixon, K.W., Gnanadesikan, A., Stouffer, R.J. and Toggweiler, J.R., 2006. The Southern Hemisphere westerlies in a warming world: Propping open the door to the deep ocean. *Journal of Climate*, *19*(24), pp.6382-6390.

Sallée, J. B., Speer, K. G., & Rintoul, S. R. (2010). Zonally asymmetric response of the Southern Ocean mixed-layer depth to the Southern Annular Mode. *Nature Geoscience*, *3*(4), 273-279.

Sen Gupta, A. and England, M.H., (2006). Coupled ocean–atmosphere–ice response to variations in the southern annular mode. *Journal of Climate*, *19*, 4457-4486

Stewart, K. D., Hogg, A. M., Griffies, S. M., Heerdegen, A. P., Ward, M. L., Spence, P., & England, M. H., (2017). Vertical resolution of baroclinic modes in global ocean models. *Ocean Modell.*, 113, 50–65, doi:10.1016/j.ocemod.2017.03.012.

Stewart, K. D., Hogg, A. M., England, M. H., and Waugh, D.W., (2020a) Response of the Southern Ocean overturning circulation to extreme Southern Annular Mode conditions, *Geophysical Research Letters*, submitted, doi: 10.1002/essoar.10503406.1

Stewart, K. D., Kim, W. M., Urakawa, S., Hogg, A. M. C., Yeager, S., Tsujino, H., Nakano, H., Kiss, A. E. & Danabasoglu, G., 2020b. JRA55-do-based repeat year forcing datasets for driving ocean–sea-ice models. *Ocean Modell.*, 147, 101557

Swart, N.C. & J.C. Fyfe, 2012: Observed and simulated changes in the Southern Hemisphere surface westerly wind-stress, *Geophys. Res. Lett.,* 39, L16711, doi:10.1029/2012GL05281

Tanhua, T., D. W. Waugh, & J. L. Bullister, 2013: Estimating changes in ocean ventilation from early 1990s CFC-12 and late 2000s SF_6 measurements, *Geophys*. *Res*. *Lett*., 40, 927–932, doi:10.1002/grl.50251.

Thompson DWJ, Solomon S, Kushner PJ, England MH, Grise KM, Karoly DJ. 2011: Signatures of the Antarctic ozone hole in Southern Hemisphere surface climate change. *Nat. Geosci.* 4, 471–479

Thompson, D. W. J., and J. M. Wallace (2000), Annular modes in the extratropical circulation: I. Month-to-month variability, *J. Climate*, 13, 1000 – 1016.

Ting, Y.H. & Holzer, M., (2017) Decadal changes in Southern Ocean ventilation inferred from deconvolutions of repeat hydrographies. *Geophysical Research Letters*.

Waugh, D.W. (2014). Changes in the ventilation of the southern oceans, *Philosophical Transactions A.,* 373, 0130269.

Waugh, D.W and Haine, T.W.N. (2020) How rapidly do the southern subtropical oceans respond to wind stress changes? *Journal of Geophys. Res.- Oceans*, to appear

Waugh, D. W., F. Primeau, T. DeVries, & M. Holzer (2013) Recent changes in the ventilation of the southern oceans, *Science*, 339, 568.

524 Waugh, D.W., A. McC. Hogg, P Spence, M. H. England, T. W.N. Haine, 2019: Response of
525 Southern Ocean ventilation to changes in mid-latitude westerly winds, *J Climate*, 32, 5345-
526 5361.

527

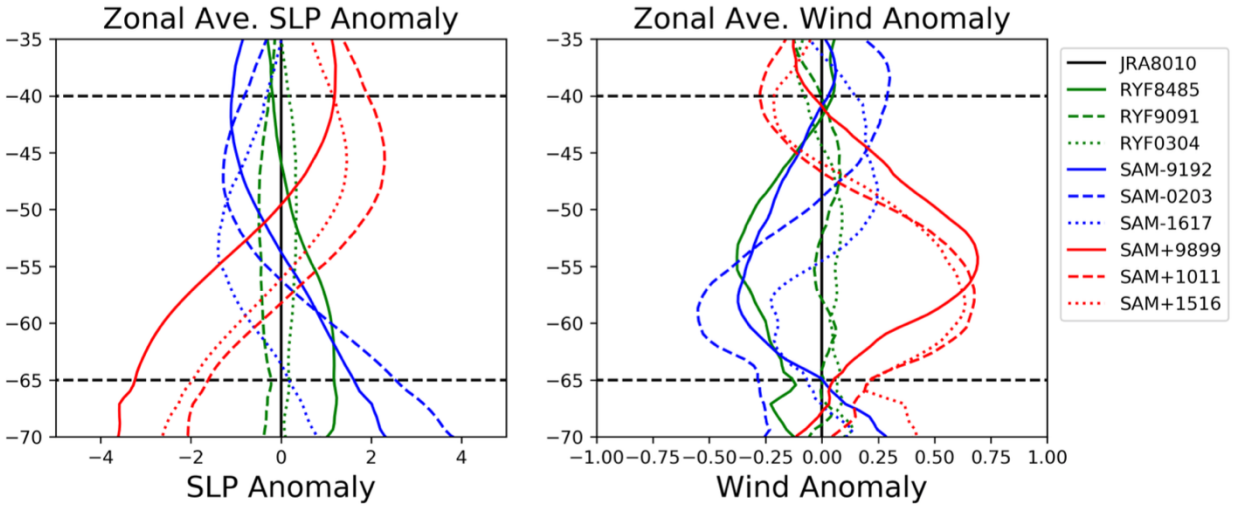

Figure 1: Latitudinal variation of anomalies in (a) sea-level pressure and (b) zonal-mean wind for different years. Green curves correspond to reference years, red to positive SAM, and blue to negative SAM.

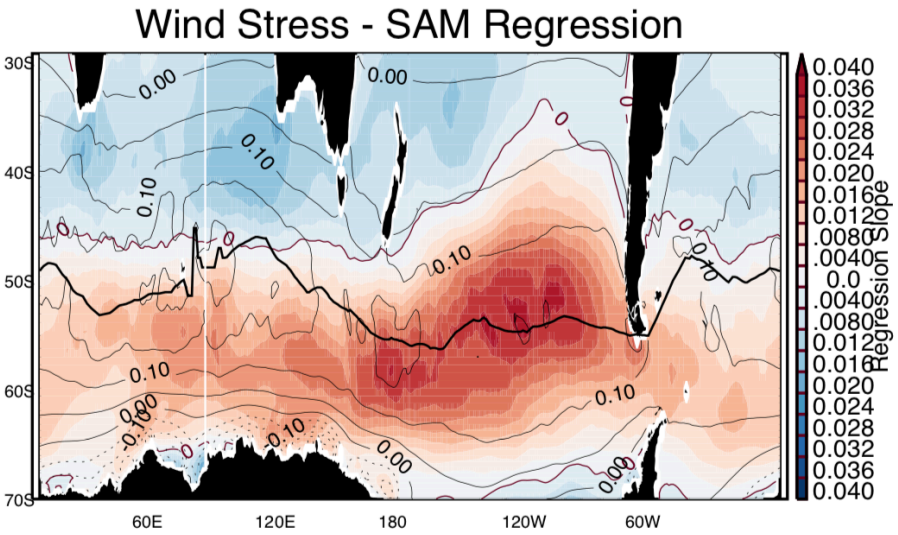

Figure 2: Map of linear regression coefficient between zonal wind stress and SAM index (N/m^2/unit SAM). Contours show climatological wind stress, and the thick curve is the location of peak wind stress.

545

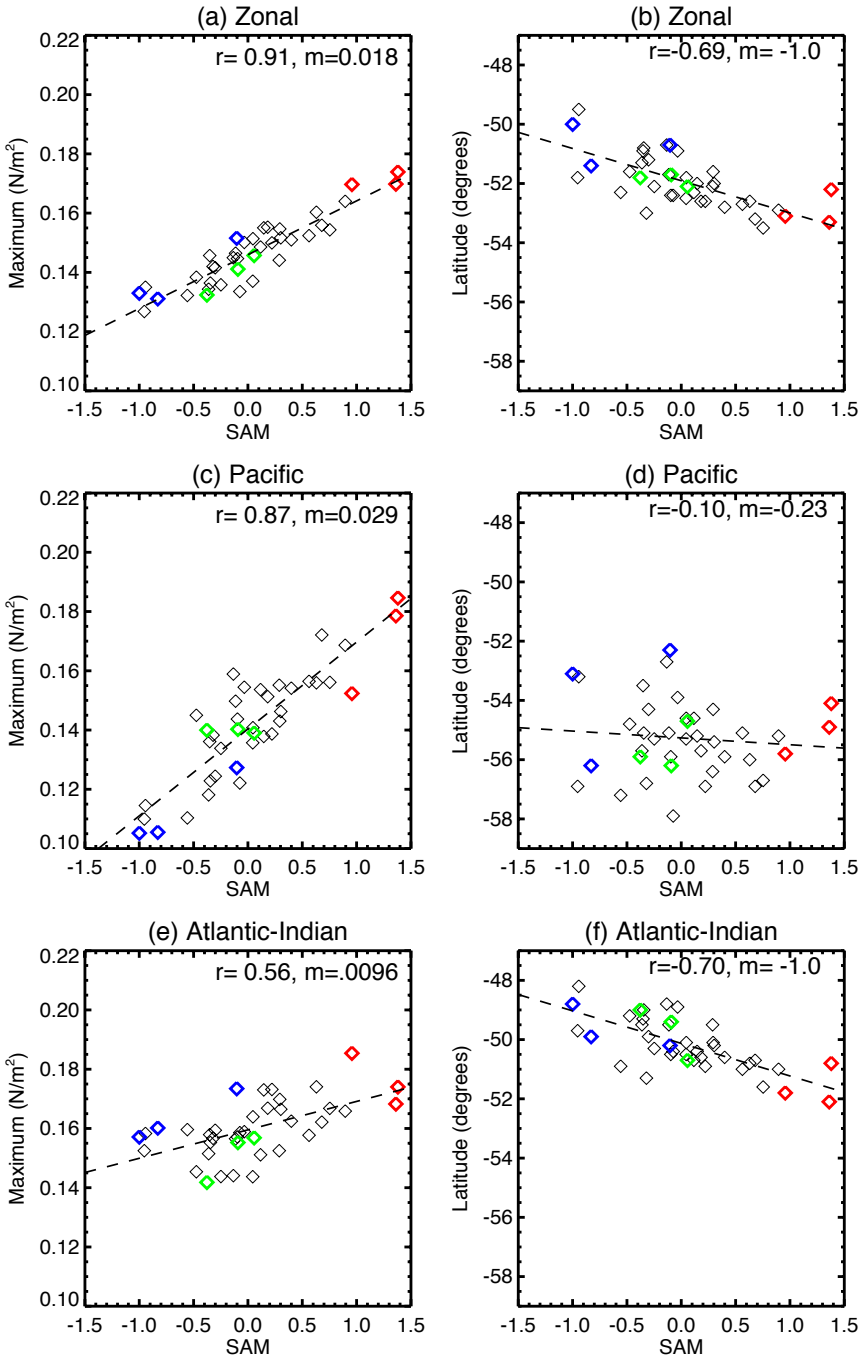

546
547 Figure 3 Scatter plots showing relationships between magnitude of peak wind stress and latitude
548 of peak wind stress with the SAM index for (a-b) zonal-mean, (c-d) Pacific-mean and (e-f)
549 Atlantic-Indian mean. Colored symbols for the RYF, SAM+ and SAM- years, as in Figure 1.
550
551

552

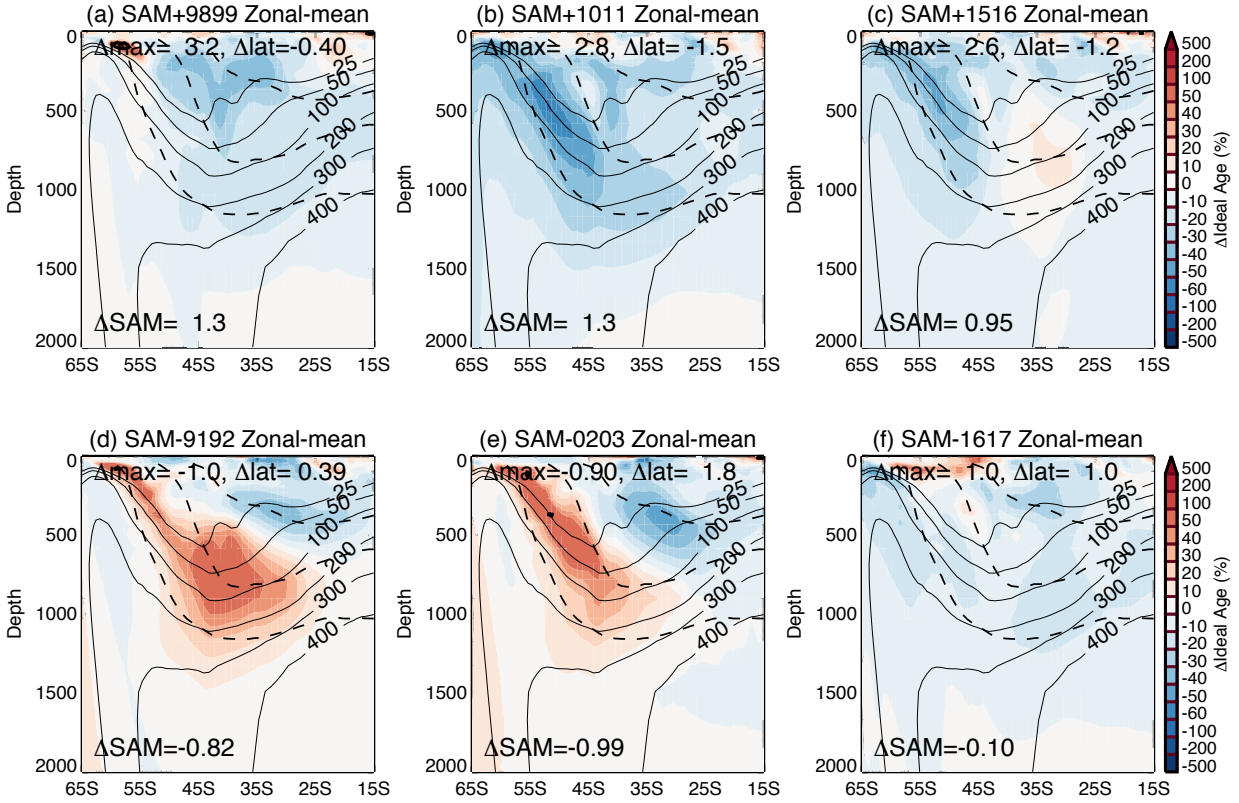

553

554 Figure 4 Depth-latitude variation of the percentage change in zonal-mean ideal age for (a-c)
555 SAM+ and (d-f) SAM- perturbations from RYF9091. Solid contours show RYF9091 ideal age,
556 and dashed contours show isopycnal surfaces. ΔSAM is the difference in SAM index between
557 perturbation and RYF simulation, Δmax the difference in maximum wind stress multipled by
558 100, and Δlat the difference in latitude of the maximum wind stress.

559

560

561

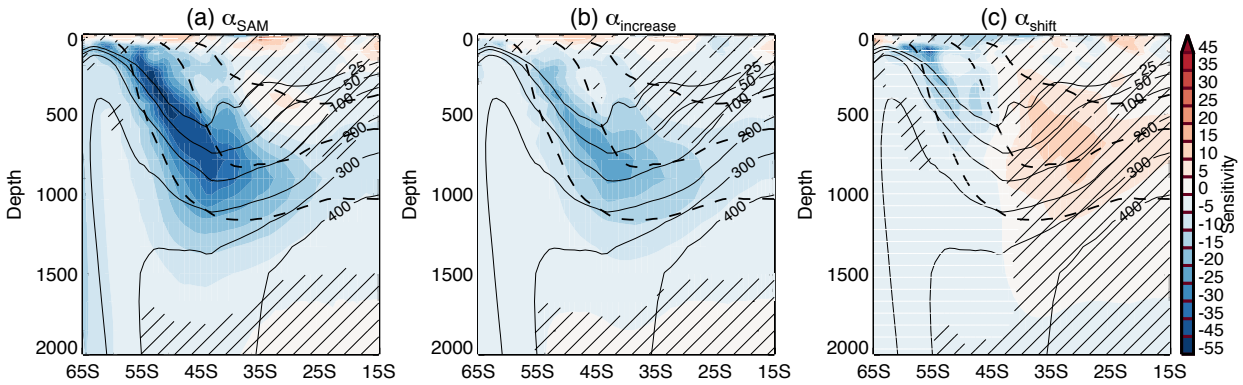

Figure 5: Depth-latitude variation of the sensitivity of the zonal-mean age to (a) an increase in SAM (α_{SAM}), (b) an increase in peak wind stress ($\alpha_{increase}$), and (c) a poleward movement of the peak wind stress (α_{shift}). Units are year/unit SAM, year/0.1N/m^2, and year/1^o for α_{SAM}, $\alpha_{increase}$, α_{shift} respectively. Contour lines as in Figure 4. Hatching indicates regions where the correlations are not significant at the 95% confidence level, using standard t-test.

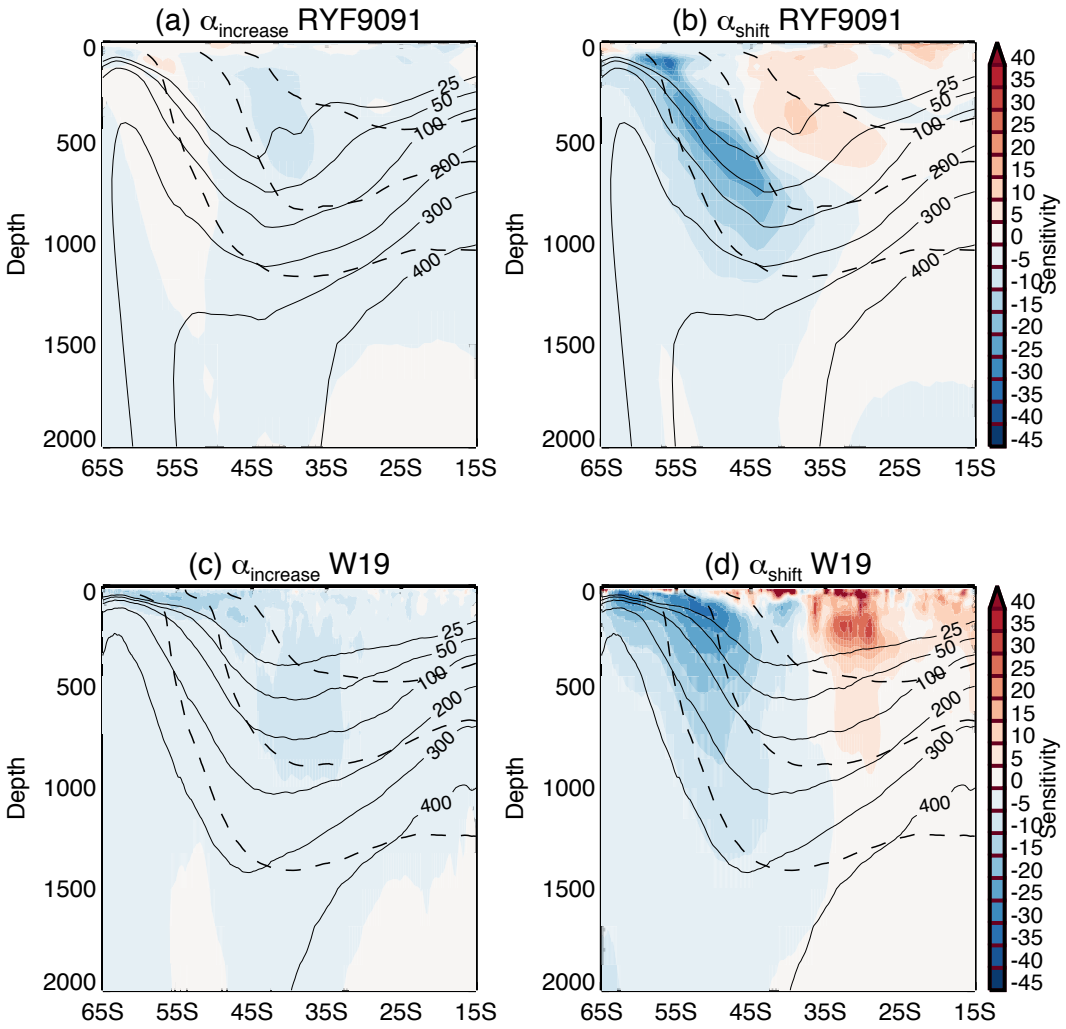

Figure 6 As in Fig 5b, c except for (a,b) RYF9091 experiments at yr 50-59, and (b) Waugh et al. (2019) wind stress perturbations.

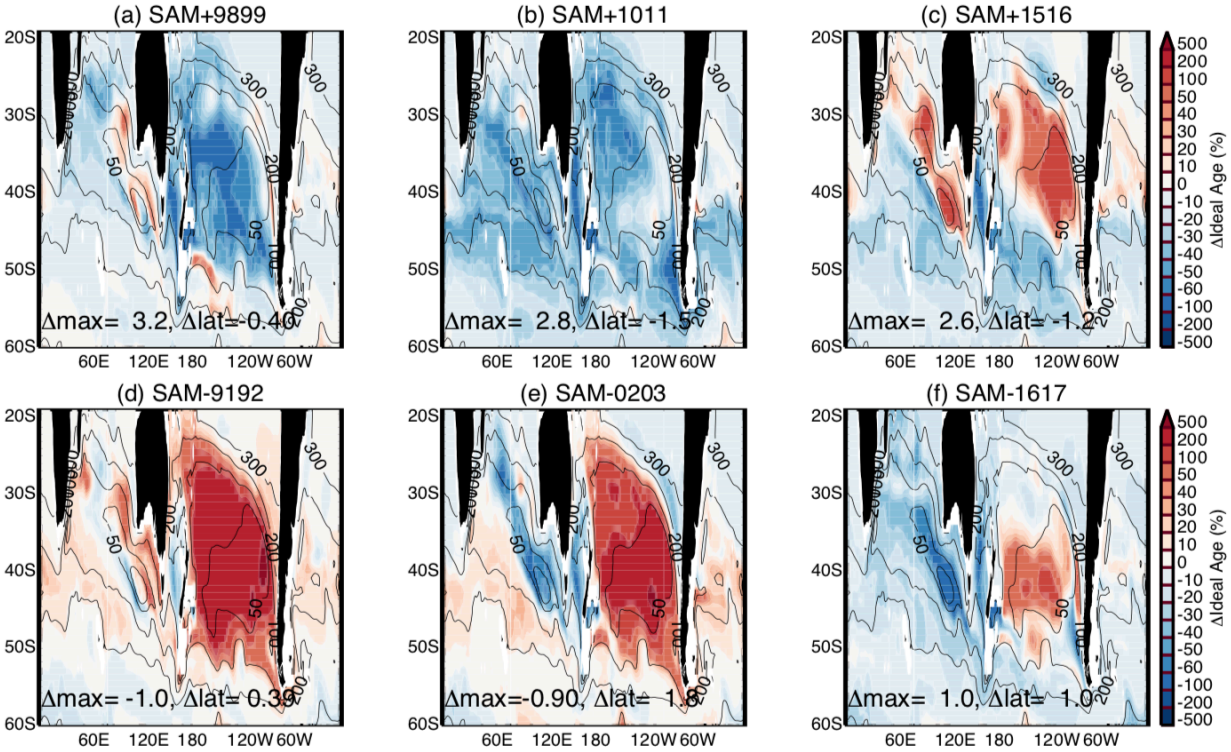

Figure 7: Maps of percentage change in age at 900 m for (a-c) SAM+ and (d-f) SAM- perturbations from RYF9091. Contours show climatological age in RYF9091. Δmax and Δlat are as defined in Figure 4.

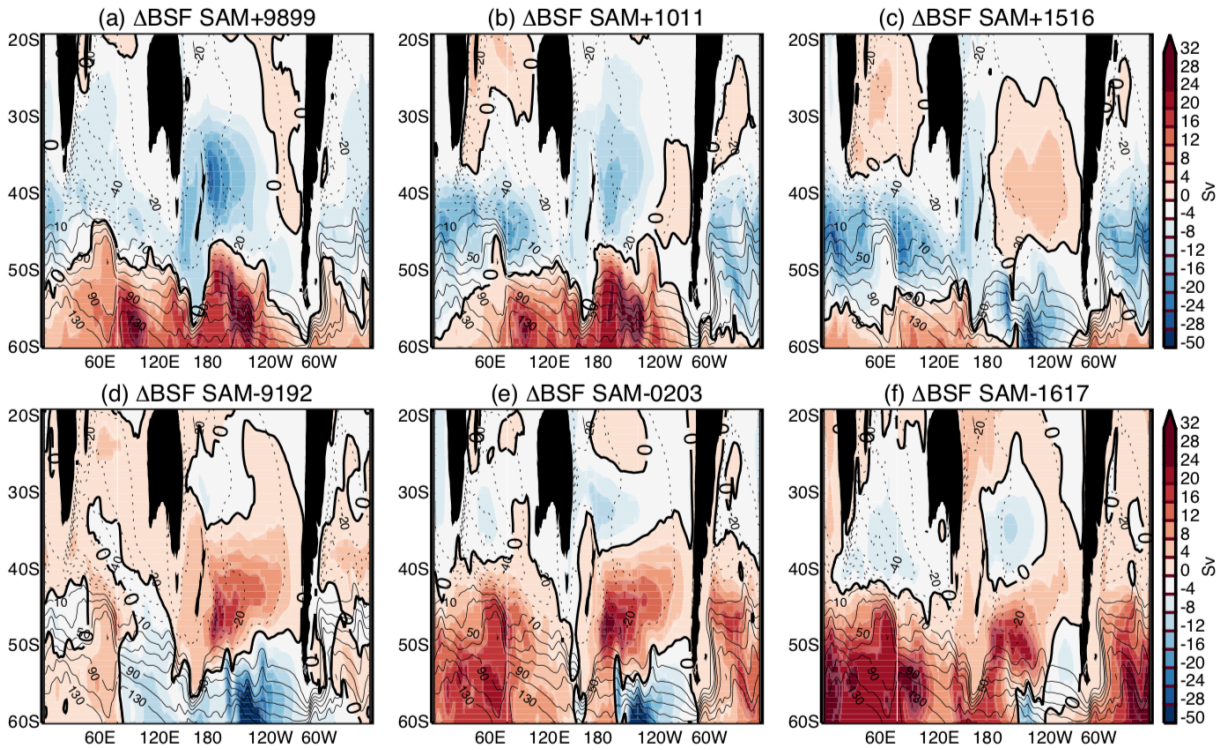

Figure 8: Maps of change in barotropic stream function (BSF) for (a-c) SAM+ and (d-f) SAM- perturbations from RYF9091. Contours show climatological BSF in RYF9091.

590

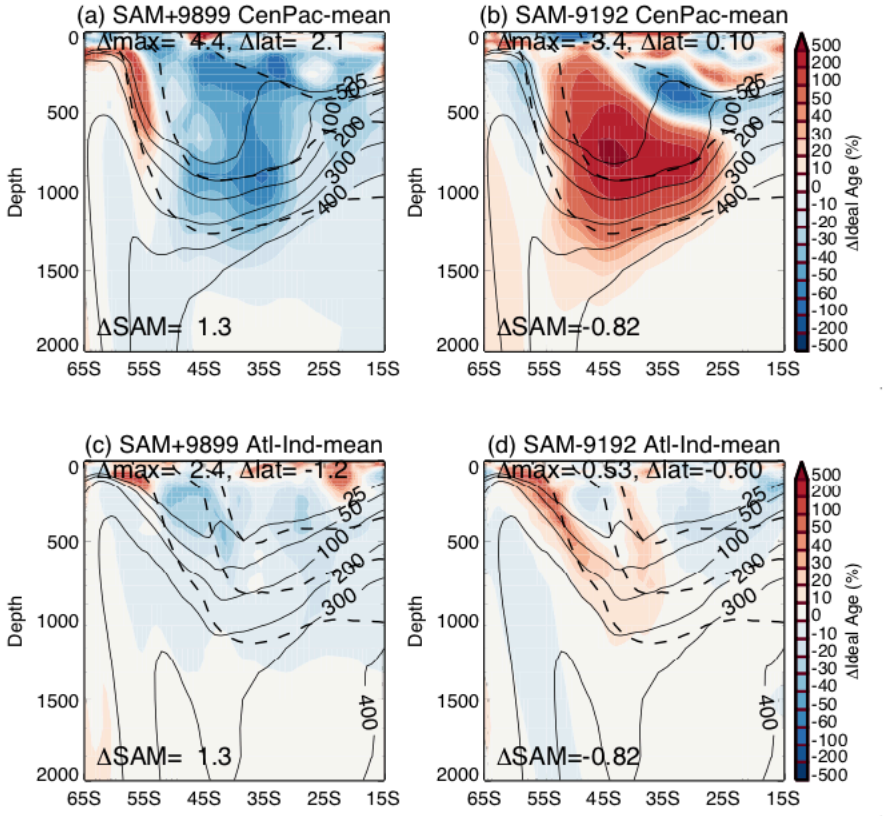

591

592 Figure 9: As in Figure 4 except for the age averaged over the (a-b) Central Pacific and (c-d)
593 Atlantic-Indian oceans, and for SAM+9899 and SAM-9192 perturbations from RYF9091.

594

595

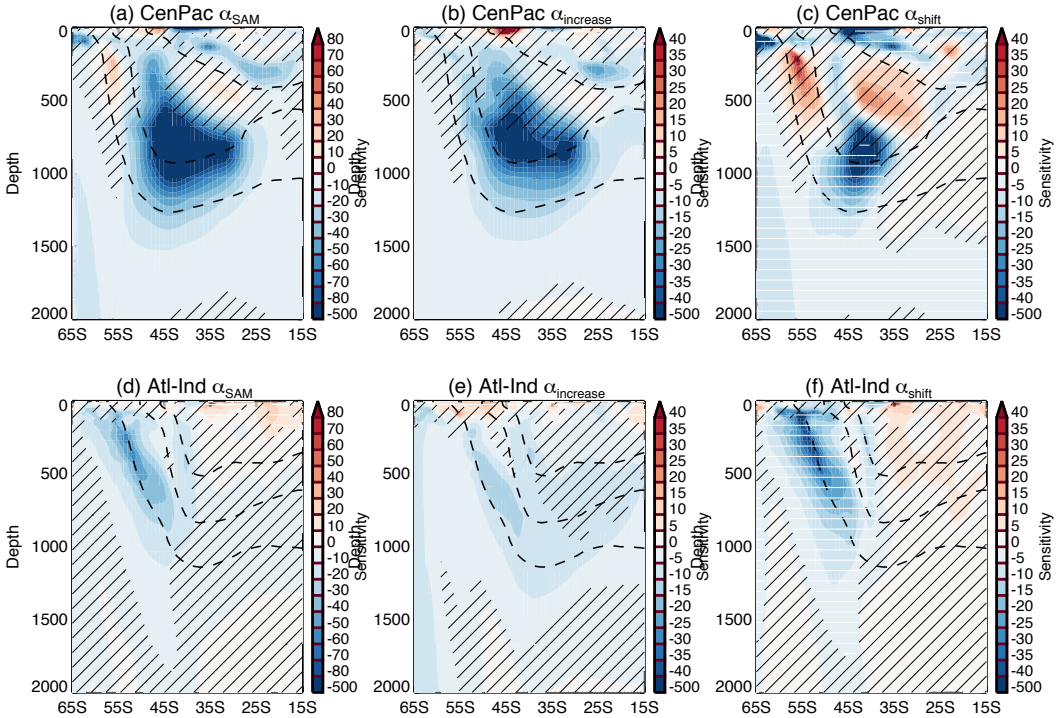

596
597 Figure 10: As in Figure 5a except for the age averaged over the (a) Central Pacific and (b)
598 Atlantic-Indian oceans.
599
600

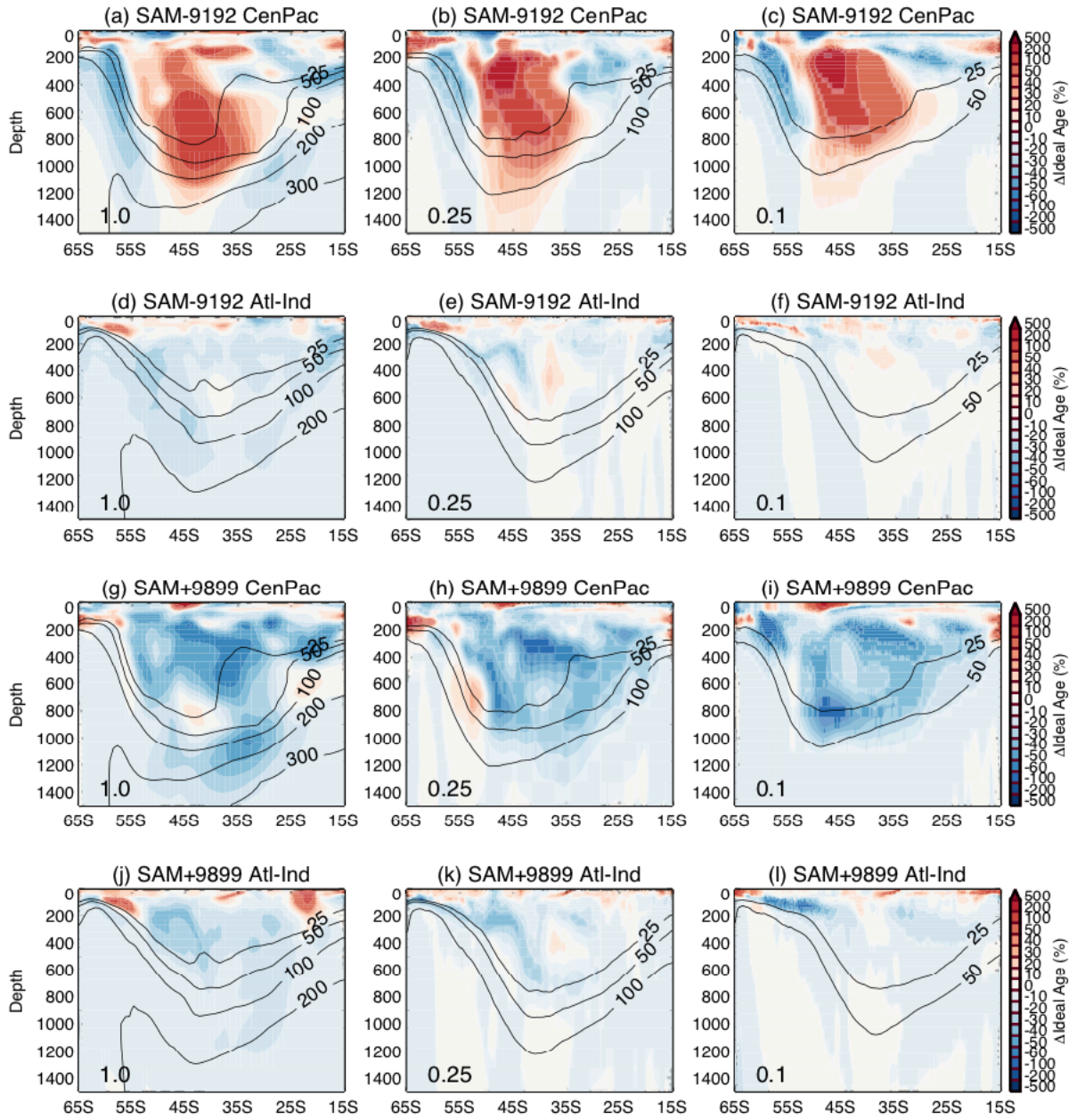

Figure 11 As in Figure 9 except showing the percentage change after 20 years for (left column) 1.0° , (middle) 0.25° and (right) 0.1° resolution simulations. Panels (a)-(f) show SAM-9192 and (g)-(l) SAM+9899 perturbations from RYF9091.